Mechanistic Studies of the Formation and Decay of Diiron(III) Peroxo Complexes in the Reaction of Diiron(II) Precursors with Dioxygen

Andrew L. Feig,[†] Michael Becker,[‡] Siegfried Schindler,[‡] Rudi van Eldik,[‡] and Stephen J. Lippard*,[†]

Department of Chemistry, Massachusetts Institute of Technology, Cambridge, Massachusetts 02139, and Institute for Inorganic Chemistry, University of Erlangen-Nürnberg, Egerlandstrasse 1, 91058 Erlangen, Germany

Received September 26, 1995[⊗]

Mechanistic studies of the reactions of three analogous alkoxo-bridged diiron(II) complexes with O_2 have been carried out. The compounds, which differ primarily in the steric accessibility of dioxygen to the diiron(II) center, form metastable μ-peroxo intermediates when studied at low temperature. At ambient temperatures, these intermediates decay to form (μ-oxo)polyiron(III) products. The effect of ligand steric constraints on the O_2 reactivity was investigated. When access to the diiron center was unimpeded, the reaction was first-order with respect to both [Fe^{II}_2] and [O_2] and the activation parameters for O_2 addition were similar to those for O_2 reacting with the dioxygen transport protein hemerythrin. When the binding site was occluded, however, reduced order with respect to [O_2] was observed and a two-step mechanism was required to explain the kinetic results. Decay of all three peroxide intermediates involves a bimolecular event, implying the formation of tetranuclear species in the transition state.

Introduction

Reduced dinuclear iron centers occur in several metalloproteins, including hemerythrin (Hr),[1−3] the R2 protein of ribonucleotide reductase (RNR) from *Escherichia coli*,[4−7] and the hydroxylase (H) component of soluble methane monooxygenase (sMMO).[8−10] In each of these systems, the diiron center is directly involved in a reaction with dioxygen that is integral to the function of the protein.[11,12] Of major interest is determining the features of these proteins which differentiate their modes of reactivity. Hr binds dioxygen, but subsequent reactions leading to cleavage of the O−O bond are disfavored. In RNR and MMO, four-electron reduction of dioxygen occurs with chemical utilization of the oxidizing equivalents. In RNR, the dioxygen reaction oxidizes Tyr-122 to a functionally important tyrosyl radical whereas, in sMMO, a substrate alkane is oxidized to an alcohol. A similarity between the RNR and MMO activities can be observed in the F208Y mutant R2 protein.[13] Exposure of the apo form of this altered enzyme to iron(II) and dioxygen converts the tyrosine residue to dihydroxyphenylalanine (DOPA).

Reactions of the reduced forms of RNR and sMMO with dioxygen occur by multistep processes.[14−21] An early step in both cases is two-electron oxidation of the diiron(II) center. This process is similar to the dioxygen-binding reaction of deoxyHr, but the resultant peroxo species in MMO and RNR differ from the η^1-hydroperoxide coordination mode found in oxyHr.[22,23] In both MMO and RNR, the peroxo species is unstable and decomposes to less well defined intermediates. In the case of MMO, a diiron(III) peroxo intermediate (H_{peroxo}) decays to an intermediate designated Q which has been postulated to be either a diferryl species or a diiron(III) center bound to two oxyl radicals.[10,15,16,20] Further spectroscopic and mechanistic work is required to define the chemical nature of this transient. In RNR, a diferric center bridged by a single radical ligand has been proposed to be the intermediate in the oxidation mechanism.[14,17−19]

[†] Massachusetts Institute of Technology.
[‡] University of Erlangen-Nürnberg.
[⊗] Abstract published in *Advance ACS Abstracts,* April 1, 1996.

(1) Kurtz, D. M., Jr.; Shriver, D. F.; Klotz, I. M. *Coord. Chem. Rev.* **1977**, *24*, 145−178.
(2) Sanders-Loehr, J. In *Iron Carriers and Iron Proteins*; Loehr, T. M., Ed.; VCH: New York, 1989; Vol. 5; pp 373−466.
(3) Stenkamp, R. E. *Chem. Rev.* **1994**, *94*, 714−726.
(4) Nordlund, P.; Sjöberg, B.-M.; Eklund, H. *Nature* **1990**, *345*, 593−598.
(5) Stubbe, J. In *Advances in Enzymology and Related Areas of Molecular Biology*; Meister, A., Ed.; John Wiley and Sons: New York, 1990; Vol. 62; pp 349−420.
(6) Fontecave, M.; Nordlund, P.; Eklund, H.; Reichard, P. In *Advances in Enzymology and Related Areas of Molecular Biology*; Meister, A., Ed.; John Wiley and Sons: New York, 1992; Vol. 65; pp 147−183.
(7) Nordlund, P.; Eklund, H. *J. Mol. Biol.* **1993**, *232*, 123−164.
(8) Rosenzweig, A. C.; Frederick, C. A.; Lippard, S. J.; Nordlund, P. *Nature* **1993**, *366*, 537−543.
(9) Lipscomb, J. D. *Annu. Rev. Microbiol.* **1994**, *48*, 371−399.
(10) Liu, K. E.; Lippard, S. J. In *Advances in Inorganic Chemistry*; Sykes, A. G., Ed.; Academic Press, Inc.: San Diego, CA, 1995; Vol. 42, pp 263−289.
(11) Que, L., Jr. In *Bioinorganic Catalysis*; Reedijk, J., Ed.; Marcel Dekker: New York, 1993; pp 347−393.
(12) Feig, A. L.; Lippard, S. J. *Chem. Rev.* **1994**, *94*, 759−805.
(13) Åberg, A.; Ormö, M.; Nordlund, P.; Sjöberg, B.-M. *Biochemistry* **1993**, *32*, 9845−9850.
(14) Bollinger, J. M., Jr.; Edmondson, D. E.; Huynh, B. H.; Filley, J.; Norton, J. R.; Stubbe, J. *Science* **1991**, *253*, 292−298.
(15) Lee, S.-K.; Nesheim, J. C.; Lipscomb, J. D. *J. Biol. Chem.* **1993**, *268*, 21569−21577.
(16) Lee, S.-K.; Fox, B. G.; Froland, W. A.; Lipscomb, J. D.; Münck, E. *J. Am. Chem. Soc.* **1993**, *115*, 6450−6451.
(17) Bollinger, J. M., Jr.; Tong, W. H.; Ravi, N.; Huynh, B. H.; Edmondson, D. E.; Stubbe, J. *J. Am. Chem. Soc.* **1994**, *116*, 8015−8023.
(18) Bollinger, J. M., Jr.; Tong, W. H.; Ravi, N.; Huynh, B. H.; Edmondson, D. E.; Stubbe, J. *J. Am. Chem. Soc.* **1994**, *116*, 8024−8032.
(19) Ravi, N.; Bollinger, J. M., Jr.; Huynh, B. H.; Edmondson, D. E.; Stubbe, J. *J. Am. Chem. Soc.* **1994**, *116*, 8007−8014.
(20) Liu, K. E.; Valentine, A. M.; Wang, D.; Huynh, B. H.; Edmondson, D. E.; Salifoglou, A.; Lippard, S. J. *J. Am. Chem. Soc.* **1995**, *117*, 10174−10185.
(21) Liu, K. E.; Valentine, A. M.; Qiu, D.; Edmondson, D. E.; Appelman, E. H.; Spiro, T. G.; Lippard, S. J. *J. Am. Chem. Soc.* **1995**, *117*, 4997−4998.
(22) Stenkamp, R. E.; Sieker, L. C.; Jensen, L. H.; McCallum, J. D.; Sanders-Loehr, J. *Proc. Natl. Acad. Sci., U.S.A.* **1985**, *82*, 713−716.
(23) Shiemke, A. K.; Loehr, T. M.; Sanders-Loehr, J. *J. Am. Chem. Soc.* **1986**, *108*, 2437−2443.

0020-1669/96/1335-2590$12.00/0 © 1996 American Chemical Society

Scheme 1

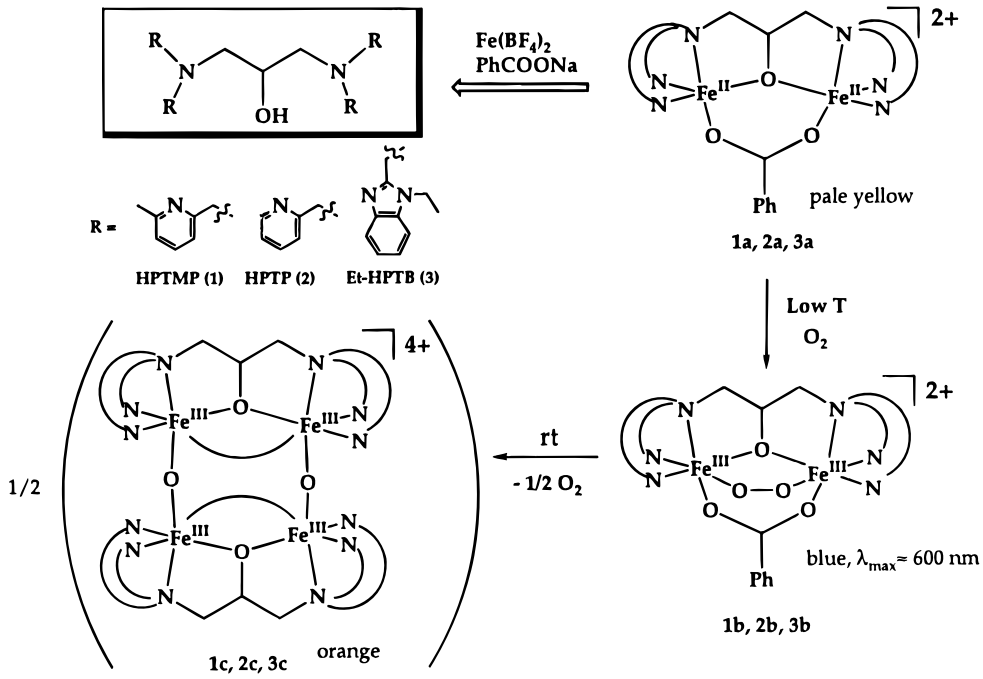

Several model compounds have been synthesized for the reduced cores of these enzymes.[24−35] Although one comes very close,[34] none is a perfect structural mimic for a protein core, and none exhibits catalytic monooxygenase activity. Several of these complexes react cleanly with dioxygen, however, to afford well-characterized products, and we have therefore undertaken a systematic investigation of the kinetics of the dioxygen reaction. Elsewhere we have described our studies with $[Fe_2(O_2CH)_4(BIPhMe)_4]$ and $[Fe_2(OH)(O_2CCH_3)_2(Me_3\text{-}TACN)_2]^+$.[51,62] In the present article, we report results for three closely related compounds, each containing a (μ-alkoxo)(μ-carboxylato)diiron(II) core coordinated by *N*,*N*′,*N*′,*N*′-tetrasubstituted-1,3-diamino-2-hydroxypropane (HPTR) ligands. The dioxygen reactivity of these compounds is of particular interest mechanistically because of the ability to isolate different phases of the reaction (Scheme 1). When first reported by other laboratories, it was noted that stable peroxide adducts formed following exposure to dioxygen at low temperature.[28,30] Spectroscopic studies of these complexes revealed the presence of a symmetrically bound peroxide, presumably coordinated in a μ-1,2 fashion. In the case of compound **1a**, dioxygen binding was reversible.[28] Once dioxygen was bound to either **2a** or **3a**, however, it could not be released.[30,36,37] Thus, although the chemical differences among **1a**−**3a** are subtle, consisting primarily of changes in the steric properties around the diiron center, the effects of these differences on the reactions with dioxygen are profound. Upon warming, all three of the metastable diferric peroxo complexes decompose, but at temperatures which vary considerably.[30] We are interested in understanding these differences, especially the structural features which influence the reactivity of the diiron(II) compounds and their activated dioxygen complexes. From this information, it should be possible to predict the chemical properties of the metastable diiron(III) peroxo species. A portion of this work has been communicated previously.[38]

Experimental Section

General Considerations. All solvents were dried and distilled prior to use.[39] For most studies, propionitrile (Fluka) was prepared by distillation from CaH_2. Significant levels of residual water were present after this treatment, as measured by Karl Fischer analysis (Galbraith Laboratories). Rigorously dry solvent, used to determine the effects of small amounts of added water, was obtained by predrying over CaH_2, decanting the solvent into a distillation flask containing P_2O_5 (5 g/L), and refluxing overnight under N_2. The propionitrile was collected by distillation and then refluxed over CaH_2 (5 g/L). After 12 h, the solvent was collected by distillation and transferred to a glovebox. Karl Fischer analysis of propionitrile treated in this manner contained <34 ppm of residual water. Dioxygen was purified by passing the gas stream through a 1 m column of Drierite. Anaerobic manipulations were carried out in a nitrogen-filled glovebox (Vacuum Atmospheres) or by using standard Schlenk techniques. Labeled dioxygen (≈98% $^{18}O_2$) was obtained from Isotech (Miamisburg, OH) and used without further purification.

(24) Hartman, J. R.; Rardin, R. L.; Chaudhuri, P.; Pohl, K.; Wieghardt, K.; Nuber, B.; Weiss, J.; Papaefthymiou, G. C.; Frankel, R. B.; Lippard, S. J. *J. Am. Chem. Soc.* **1987**, *109*, 7387−7396.
(25) Borovik, A. S.; Que, L., Jr. *J. Am. Chem. Soc.* **1988**, *110*, 2345−2347.
(26) Kitajima, N.; Fukui, H.; Moro-oka, Y.; Mizutani, Y.; Kitagawa, T. *J. Am. Chem. Soc.* **1990**, *112*, 6402−6403.
(27) Tolman, W. B.; Liu, S.; Bentsen, J. G.; Lippard, S. J. *J. Am. Chem. Soc.* **1991**, *113*, 152−164.
(28) Hayashi, Y.; Suzuki, M.; Uehara, A.; Mizutani, Y.; Kitagawa, T. *Chem. Lett.* **1992**, 91−94.
(29) Stassinopoulos, A.; Schulte, G.; Papaefthymiou, G. C.; Caradonna, J. P. *J. Am. Chem. Soc.* **1991**, *113*, 8686−8697.
(30) Dong, Y.; Menage, S.; Brennan, B. A.; Elgren, T. E.; Jang, H. G.; Pearce, L. L.; Que, L., Jr. *J. Am. Chem. Soc.* **1993**, *115*, 1851−1859.
(31) Hagen, K. S.; Lachicotte, R.; Kitaygorodskiy, A.; Elbouadili, A. *Angew. Chem.* **1993**, *105*, 1404−1406.
(32) Zang, Y.; Elgren, T. E.; Dong, Y.; Que, L., Jr. *J. Am. Chem. Soc.* **1993**, *115*, 811−813.
(33) Kitajima, N.; Tamura, N.; Amagai, H.; Fukui, H.; Moro-Oka, Y.; Mizutani, Y.; Kitagawa, T.; Methur, R.; Heerwegh, K.; Reed, C. A.; Randall, C. R.; Que, L., Jr.; Tatsumi, K. *J. Am. Chem. Soc.* **1994**, *116*, 9071−9085.
(34) Herold, S.; Pence, L. E.; Lippard, S. J. *J. Am. Chem. Soc.* **1995**, *117*, 6134−6135.
(35) Coucouvanis, D.; Reynolds, R. A., III; Dunham, W. R. *J. Am. Chem. Soc.* **1995**, *117*, 7570−7571.
(36) Menage, S.; Brennan, B. A.; Juarez-Garcia, C.; Münck, E.; Que, L., Jr. *J. Am. Chem. Soc.* **1990**, *112*, 6423−6425.
(37) Brennan, B. A.; Chen, Q.; Juarez-Garcia, C.; True, A. E.; O'Connor, C. J.; Que, L., Jr. *Inorg. Chem.* **1991**, *30*, 1937−1943.
(38) Feig, A.; Lippard, S. J. *J. Am. Chem. Soc.* **1994**, *116*, 8410−8411.
(39) Perrin, D. D.; Armarego, W. L. F. *Purification of Laboratory Chemicals*, 3rd ed.; Butterworth-Heinemann: Oxford, U.K., 1988.

Ligand Syntheses. The compound *N*,*N*,*N*′,*N*′-tetrakis[(6-methylpyrid-2-yl)methyl]-2-hydroxy-1,3-diaminopropane (HPTMP) (**1**),[28] was synthesized by a new method described below. The other ligands, *N*,*N*,*N*′,*N*′-tetrakis(2-pyridylmethyl)-2-hydroxy-1,3-diaminopropane (HPTP) (**2**) and *N*,*N*,*N*′,*N*′-tetrakis[(*N*-ethyl-2-benzimidazolyl)methyl]-2-hydroxy-1,3-diaminopropane (Et-HPTB) (**3**), were prepared according to literature procedures.[30]

6-Methyl-2-(hydroxymethyl)pyridine. To a solution of 6-methyl-2-pyridinecarboxaldehyde (25.0 g, 0.207 mol) in ethanol (100 mL) at 0 °C was added 3.0 g of $NaBH_4$. The solution was stirred for 1 h, after which 100 mL of H_2O was added. The solution was neutralized by addition of 1.0 M aqueous HCl, and the product was extracted into Et_2O. The solution was dried over $MgSO_4$ and the solvent removed under reduced pressure, yielding the product alcohol as a colorless oil (23.2 g, 0.189 mol, 91.5%). ^{1}H NMR (300 MHz, $CDCl_3$): δ 7.56 (t, 1 H, J = 7.5 Hz), 7.05 (apparent t, 2 H, J = 7.8 Hz), 4.71 (s, 2 H), 2.54 (s, 3 H).

6-Methyl-2-(bromomethyl)pyridine. The above alcohol was dissolved in 70 mL of 48% HBr. Concentrated H_2SO_4 (50 mL) was added slowly, and the solution was refluxed overnight. The reaction mixture was poured into 100 mL of H_2O and then neutralized with saturated aq Na_2CO_3. The product was extracted into Et_2O and dried over $MgSO_4$. The solvent was removed under reduced pressure, yielding a pink solid (29.0 g, 0.156 mol, 82.5%). ^{1}H NMR (250 MHz, $CDCl_3$): δ 7.57 (t, 1 H, J = 7.8 Hz), 7.23 (d, 1 H, J = 7.8 Hz), 7.05 (d, 1 H, J = 7.8 Hz), 4.51 (s, 2 H), 2.55 (s, 3H). EI MS: *m/z* 185, 187 (isotope ratio 1:1, M^+).

***N*,*N*,*N*′,*N*′-Tetrakis[(6-methylpyrid-2-yl)methyl]-2-hydroxy-1,3-diaminopropane.** To a solution of 1,3-diamino-2-propanol (0.902 g, 10 mmol) in H_2O (25 mL) were added (6-methylpyrid-2-yl)methyl bromide (8.60 g, 46 mmol) and NaOH (4.5 g, 113 mmol). The solution was refluxed overnight, and upon cooling, a biphasic mixture was obtained. The organic component was extracted three times into CH_2Cl_2, the extract was dried over $MgSO_4$, and the solvent was removed under reduced pressure. The product was purified by silica column chromatography (EtOAc/MeOH), yielding a viscous brown oil (3.73 g, 9.03 mmol). ^{1}H NMR (250 MHz, $CDCl_3$): δ 7.45 (apparent t, 4 H, J = 7.7 Hz), 7.17 (d, 4 H, J = 7.8 Hz), 6.93 (d, 4 H, J = 7.5 Hz), 3.90 (m, 1 H), 3.80 (dd, 4 H, J = 6.0 and 37.5 Hz), 2.45−2.62 (m, 8 H), 2.46 (s, 12 H). This spectrum matches that previously reported for material prepared by an alternative route.[28] The overall three step yield was 68.2%.

Preparation of Iron(II) Compounds. The three complexes used in this study, $[Fe_2(HPTMP)(OBz)](BPh_4)_2$ (**1a**), $[Fe_2(HPTP)(OBz)](BPh_4)_2$ (**2a**), and $[Fe_2(Et\text{-}HPTB)(OBz)](BF_4)_2$ (**3a**), were synthesized by methods previously reported[28,30] and purified by multiple (usually three) recrystallizations from acetonitrile by vapor diffusion of Et_2O under a nitrogen atmosphere.

Optical Absorption Spectra. Electronic spectral properties of compounds **1b**−**3b** were previously reported.[28,30] Prior to beginning kinetic work, we recollected these spectra using a Hewlett Packard 8452A diode array instrument fitted with a specially modified Dewar flask with quartz windows. Absorptions due to the metastable dioxygen adducts were observed at −77 °C. Values for the extinction coefficients were determined on the basis of a Beer's law analysis of parameters obtained by curve fitting of the results of the kinetic experiments carried out in dry solvent. The values matched those measured in static oxygenation experiments. Extinction coefficients were assumed not to vary with temperature.

Manometry. Manometric experiments were carried out in propionitrile as described previously,[27] but with minor modifications. Because of the temperature sensitivity of the peroxide intermediates, dioxygen uptake for the first phase of the reaction was measured with the reaction flask cooled to −77 °C by immersion in a dry ice/acetone bath. After equilibrium was achieved, decomposition of the peroxide was measured by warming the reaction vessel to 22 °C. Dioxygen consumption was measured manometrically at least twice and is reported as the mean of the values.

Dioxygen Isotope Exchange Studies. To determine whether oxygen atom exchange occurred during the decomposition of **3b** to **3c**, 50 mg samples of **3a** dissolved in propionitrile were prepared in separate reaction flasks and cooled to −77 °C. The samples were oxygenated with either $^{16}O_2$ or $^{18}O_2$, and both flasks were purged of excess O_2 by repeated vacuum/argon cycling. The $^{18}O_2$ sample was then transferred by cannula to the flask containing the unlabeled material. The head space above the reaction mixture was evacuated by using a modified Toepler pump (Figure 1) while the sample was kept cold. This process involves preevacuation of the pump by opening valves 1, 2, 3, and 5. Valves 1 and 3 were then closed, and valve 4 was opened. With the valves in this setting, gas from the reaction flask was pumped into the collection tube, the pumping speed being controlled by partially opening valve 6. This procedure was repeated until no O_2 was detected in the collection tube. The reaction flask was then isolated from the pump by closing valve 4, and the solution was stirred at room temperature under vacuum for 2 h, at which time the decay of the peroxo species was over, on the basis of the complete discharge of the blue color. The pump was pre-evacuated as just described, and valve 4 was opened. Gas collected in the receiving tube connected to the outlet of the Toepler pump was then analyzed by mass spectrometry (Hewlett Packard 5971 mass spectrometer).

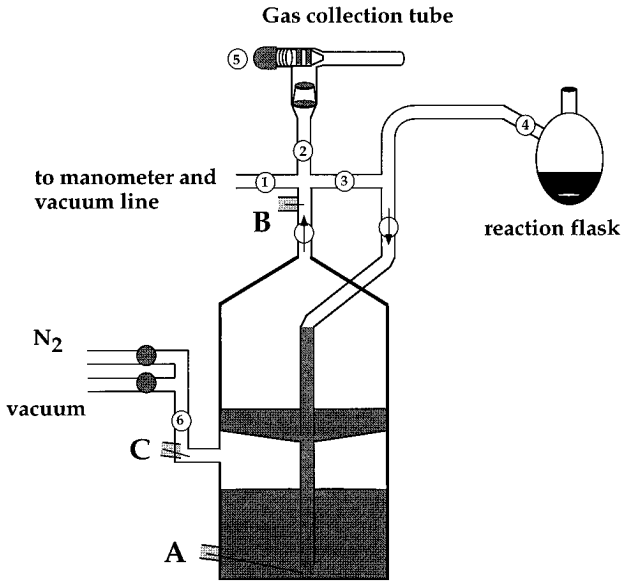

Figure 1. Schematic drawing of the Toepler pump used in the isotope-labeling studies. Open circles represent manual control valves. Shaded circles represent solenoids controlled by the electronic relay, and A, B, and C are contacts used by the relay circuit. Circles with arrows are one-way valves in the directions indicated.

Stopped-Flow Kinetics Experiments. All ambient-pressure kinetics experiments were carried out by using a Canterbury SF-41 stopped-flow instrument (Hi-Tech) and a specially assembled fiber-optics spectrometer (components from Oriel Corp.). It consisted of a visible light source (quartz−halogen lamp, 100 W) irradiating a monochromator ($^1/_8$ m, holographic grating 1200 lines/mm, blazed at 200 nm) connected to a fused-silica fiber-optics bundle. The monochromatic light was focused on the stopped-flow cell. A second fiber-optics bundle collected the transmitted light and irradiated a photomultiplier tube (Oriel 77341). Data were collected through software developed locally (Labview2 environment, National Instruments, Apple Macintosh IIfx computer) at a sampling rate such that approximately 1000 points were acquired over the course of the reaction with a linear time base. The effect of pressure on the formation of the peroxide intermediate **3b** was measured as described elsewhere.[40] The preferred solvent for these studies was propionitrile because of its low freezing (−95 °C) and high boiling (97 °C) points and was used unless noted otherwise. The formation of intermediates **1b**−**3b** was studied under pseudo-first-order conditions with excess of O_2. Concentrations of the ferrous complexes varied from 0.02 to 0.50 mM, and the dioxygen concentration at saturation (20 °C) was 8.8 mM.[41] Saturation concentrations in other solvents were calculated from the Ostwald coefficients (L) and

(40) van Eldik, R.; Gaede, W.; Wieland, S.; Kraft, J.; Spitzer, M.; Palmer, D. A. *Rev. Sci. Instrum.* **1993**, *64*, 1355−1357.

eq 1, where X is the mole fraction, R is the gas constant, T is the

$$X = \left(\frac{RT}{P_{(g)}LV^{\circ}_{(l)}} + 1\right)^{-1} \quad (1)$$

temperature, $P_{(g)}$ is the partial pressure, and $V^{\circ}_{(l)}$ is the molar volume.[42] Dioxygen concentrations were varied over the 0.8−4.4 mM range at room temperature. A linear correction for the contraction of propionitrile as a function of temperature was previously measured[41] and is given in eqs 2 and 3. This correction was applied to the dioxygen

$$\rho = 0.8011(4) - 0.0009801(90)T \quad (T \text{ in } ^{\circ}\text{C}) \quad (2)$$

$$[O_2]_T = \frac{[O_2]_{22^{\circ}C}}{\rho_{22^{\circ}C}}\rho_T \quad (3)$$

concentration whenever the rate constant depended upon this value. Once it was determined that the decay phase of the reaction was not $[O_2]$-dependent, the reaction conditions for these runs were varied beyond the pseudo-order limits, employing complex concentrations as high as 1.0 mM.

Rate constants were derived from optical traces obtained at 600 nm, a wavelength at which both the formation and the decomposition of the peroxide intermediate can be observed. The data were analyzed with Kaleidagraph (Abelbeck Software) running on a Macintosh IIfx computer and fit to model-dependent equations by nonlinear least-squares regression. The formation and decay phases of the reaction were studied independently by varying the temperature and time base. Traces used for curve fitting were all recorded to at least 3 half-lives. For the formation of the peroxo species, optical density data were fit to eq 4, a generalized first-order growth expression, where A_t is the

$$A_t = A_\infty + (\Delta A)(1 - \exp(-k_{obs}t)) \quad (4)$$

absorbance at time t, A_∞ is the absorbance at infinite time, and ΔA is the change in absorbance during the reaction. Errors provided for the kinetic constants are based on the standard deviation from the mean for multiple runs under identical conditions. Errors for the activation parameters are based on the propagated errors from the linear fit of the Eyring plot or plot of ln(k) vs pressure. Beer's law analysis of the fitting parameters allowed the determination of the extinction coefficients at 600 nm for **1b**−**3b**. These values were used to convert the optical density to concentration prior to the curve fitting of decay traces to eq 5, where $[\mathbf{B}]_t$ is the concentration of **B** at time t, $[\mathbf{B}]_\infty$ is the final concentration of **B**, and $\Delta[\mathbf{B}]$ is the change in the concentration of **B** during the reaction. Under certain conditions for compound **1a**, both the formation and decay could be observed with the same time base. Such data could be fit to the sum of a first-order growth and a second-order decay (eq 6). Omission of the initial growth phase and refitting

$$[\mathbf{B}]_t = [\mathbf{B}]_\infty + \frac{1}{\frac{1}{\Delta[\mathbf{B}]} + k_{obs}t} \quad (5)$$

$$[\mathbf{B}]_t = [\mathbf{B}]_\infty + (\Delta[\mathbf{B}])(1 - \exp(k_{1,obs})) + \frac{1}{\frac{1}{\Delta[\mathbf{B}]} + k_{2,obs}t} \quad (6)$$

the data to a simple second-order decay yielded identical rate constants. Under conditions of incomplete separation of the first and second phases of the reaction, kinetic results for the decay reaction are reported as fits of eq 5 to the decay phase of the experimental trace. This analysis allowed accurate fitting of the traces with fewer independent variables.

Reactions performed under strictly anhydrous conditions were used to provide zero points prior to studies of the effect of added water on the oxidation rates. Procedures for these experiments were slightly altered to ensure a minimum amount of residual water. Prior to these experiments, THF solutions of sodium benzophenone ketyl were passed through the flow lines until the blue color showed no loss in intensity over a 6 min period. The residual ketyl was then flushed from the system with a small volume of dry THF and then dry EtCN. The experiments were run immediately thereafter. Solvents for these experiments were freshly distilled as discussed above. Oxygenated water was added to the oxygenated propionitrile solution just prior to reaction with the dry, anaerobic iron solution.

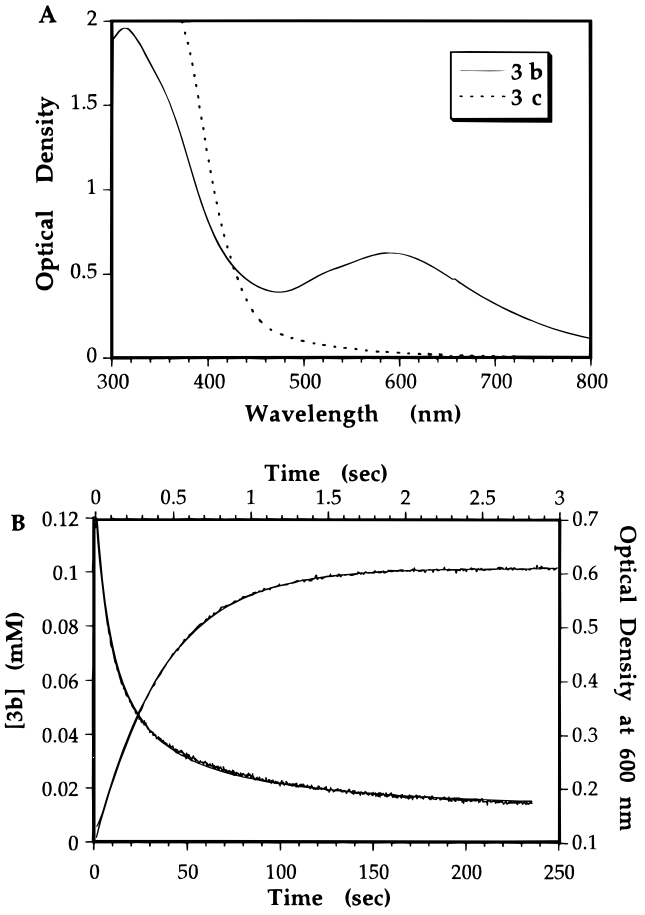

Figure 2. (A) Optical spectra of **3b** and **3c** in EtCN. (B) Sample kinetic traces for the growth (top and right axes) and decay (left and bottom axes) of **3b**. Experimental traces are overlaid by a least-squares fit of the data to the equations given in the text. Growth phase conditions: −55 °C, 0.40 mM **3a**, 4.52 mM O_2. Decay phase conditions: 55 °C, 0.125 mM **3a**, 4.21 mM O_2.

Results

Oxygenation of the Diferrous Complexes 1a−3a. The reaction of compounds **1a**−**3a** with dioxygen at low temperature leads to the formation of **1b**−**3b**, diferric species presumed to contain a symmetrically bridging peroxide ligand. Previous spectroscopic studies of these complexes are consistent with either a μ-η^1:η^1 or a μ-η^2:η^2 geometry, although the former is preferred on the basis of the 875−900 cm^{-1} O−O stretching frequencies observed in the Raman spectra.[30] This structure has now been confirmed crystallographically in two related complexes.[43] The reaction was followed by monitoring a peroxide-to-iron charge transfer band, a broad feature centered near 600 nm for all three complexes (Figure 2A). When studied under conditions of excess dioxygen, simple first-order kinetic traces were observed for the buildup of the peroxide intermediates (Figure 2B).

(41) Karlin, K. D.; Wei, N.; Jung, B.; Kaderli, S.; Niklaus, P.; Zuberbühler, A. D. *J. Am. Chem. Soc.* **1993**, *115*, 9506−9514.

(42) *Oxygen and Ozone*; Battino, R., Ed.; Pergamon Press: Oxford, U.K., 1981; Vol. 7.

(43) While this work was being reviewed, we learned of two X-ray structural analyses of related (μ-1,2-peroxo)diiron(III) complexes: Ookubo, T.; Sugimoto, H.; Nagayama, T.; Masuda, H.; Sato, T.; Tanaka, K.; Maeda, Y.; Okawa, H.; Hayashi, Y.; Uehara, A.; Suzuki, M. *J. Am. Chem. Soc.* **1996**, *118*, 701−702. Dong, Y.; Yan, S.; Young, V. G. Jr.; Que, L. Jr. *Angew. Chem.* **1996**, in press.

Table 1. Manometric Studies of the Dioxygen Uptake of **1a**−**3a**[a]

compd	peroxide formn reacn	peroxide decay reacn
1a	n.d.[b]	0.60 ± 0.10
2a	0.87 ± 0.10	0.45 ± 0.10
3a	0.80 ± 0.10[c]	0.40 ± 0.10

[a] In equivalents based on the amount of diiron(II) sample used in the experiment. $T = -77$ °C unless stated otherwise for the formation and 22 °C for the decay reaction. [b] Previously measured to be 1.0.[30] [c] Measured at −25 °C.

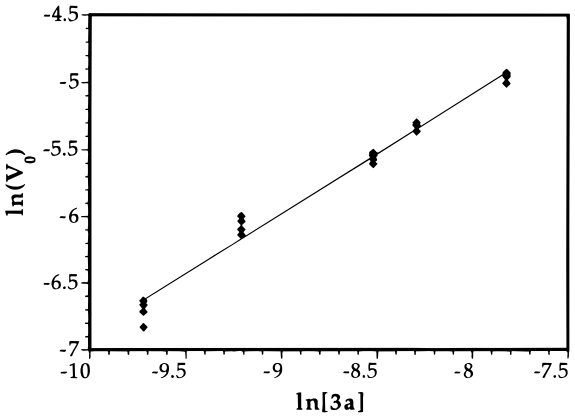

Figure 3. Plot of $\ln(V_0)$ versus $\ln([\mathbf{3a}])$ (0.05−0.50 mM) used to determine the reaction order with respect to complex for the formation of **3b**. The slope of the linear regression corresponds to the reaction order.

Rate constants were derived from time-dependent absorbance changes by using a nonlinear least-squares fitting procedure described in the Experimental Section. Extinction coefficients at 600 nm for **1b**−**3b** of 1550 ± 58, 1559 ± 41, and 1421 ± 22 M^{-1} cm^{-1}, respectively, derived from the fitting parameters agree with those obtained by a Beer's law analysis of the low-temperature spectra (see Experimental Section). These values were used to convert molar absorbances to concentrations for the determination of initial rates and for curve fitting of the second-order decay phase of the reaction, discussed below. Manometric analysis at low temperature verified the previously reported 1:1 stoichiometry for the reactions forming **2b** and **3b** (Table 1).[28,30]

Experimental Rate Laws for the Formation of 1b−**3b.** Kinetic runs were made by varying the complex concentrations over the range 0.05−0.50 mM. A plot of $\ln(V_0)$ versus $\ln([\mathbf{3a}])$ is depicted in Figure 3 (see also Table S1). (Note: Throughout, "S" preceding the number of a table or a figure indicates Supporting Information.) The reaction was first-order (0.9−1.0 ± 0.1) with respect to complex in all cases. When the $[O_2]$ was varied, however, different behavior was observed for **1a** compared to the other two compounds. Clean first-order behavior with respect to dioxygen concentration (Tables S2−S4) was exhibited by **2a** and **3a**. The mechanism and rate law for the formation of **2b** and **3b** are therefore as described by eqs 7 and 8, respectively. A partial order with respect to dioxygen, 0.65 ± 0.10, was measured for the reaction of **1a**, indicating that the mechanism is more complicated. Two mechanisms can explain this reduced order in O_2, as shown in eqs 9−14. Rate laws corresponding to these reaction schemes are provided in eqs 11 and 14.

$$\mathbf{A} + O_2 \xrightarrow{k_1} \mathbf{B} \tag{7}$$

$$\frac{d[\mathbf{B}]}{dt} = k_1[\mathbf{2a},\mathbf{3a}][O_2] \tag{8}$$

$$\mathbf{1a} \underset{k_{-0}}{\overset{k_0}{\rightleftharpoons}} \mathbf{1a'} \tag{9}$$

$$\mathbf{1a'} + O_2 \xrightarrow{k_1'} \mathbf{1b} \tag{10}$$

$$\frac{d[\mathbf{B}]}{dt} = \frac{k_0 k_1'[\mathbf{1a}][O_2]}{k_{-0} + k_1'[O_2]} \tag{11}$$

$$\mathbf{1a} + O_2 \underset{k_{-0}}{\overset{k_0}{\rightleftharpoons}} \mathbf{1a}{\cdot}O_2 \tag{12}$$

$$\mathbf{1a}{\cdot}O_2 \xrightarrow{k_1'} \mathbf{1b} \tag{13}$$

$$\frac{d[\mathbf{B}]}{dt} = \frac{k_1' K_0[\mathbf{1a}][O_2]}{1 + K_0[O_2]} \tag{14}$$

Reactions following the simple one-step addition (eq 7) can be differentiated from those undergoing two-step mechanisms (eqs 9 and 10 and eqs 12 and 13) by plotting $(k_{obs})^{-1}$ vs $[O_2]^{-1}$, as indicated by eqs 15−17, respectively. The $(k_{obs})^{-1}$ vs $[O_2]^{-1}$ plot for the simpler reaction (eq 7) has a zero intercept at all temperatures whereas, for the other two cases, the intercept of the plot corresponds to $(k_0)^{-1}$ or $(k_1')^{-1}$. Since the rate constants are temperature-dependent, so too will be the intercept. Plots of $(k_{obs})^{-1}$ vs $[O_2]^{-1}$ for **1a**−**3a** are shown in Figure 4 (see also Tables S5−S7). These experiments clearly show that the dioxygen reactivity of **1a** differs from those of **2a** and **3a**. Compound **1a** must react by one of the two-step mechanisms. The results shown in Figure 4 cannot differentiate these two possibilities, however.

$$\frac{1}{k_{obs}} = \frac{1}{k_1[O_2]} \tag{15}$$

$$\frac{1}{k_{obs}} = \frac{1}{k_0} + \frac{1}{K_0 k_1'[O_2]} \tag{16}$$

$$\frac{1}{k_{obs}} = \frac{1}{k_1'} + \frac{1}{K_0 k_1'[O_2]} \tag{17}$$

Activation Parameters for the Oxygenation of 1a−**3a.** The temperature dependence of the reactions of **1a**−**3a** with O_2 was investigated between −75 and +20 °C. An Eyring plot (Figure 5 and Tables S8−S10) of these data provided the activation parameters listed in Table 2. The results for the three compounds fall into two categories, divided as previously noted for the experimental rate laws. Compounds **2a** and **3a** have almost identical activation parameters, $\Delta H^{\ddagger} = 16$ kJ mol^{-1} and $\Delta S^{\ddagger} \approx -120$ J mol^{-1} K^{-1}.[20,44−47]

The rate constant for oxygenation of **1a** has a dramatically different temperature dependence, reinforcing the contrast between the reaction mechanisms for this compound compared to the other two. The enthalpic contribution to the activation barrier is almost 3 times greater than those for **2a** and **3a**. The

(44) Petrou, A. L.; Armstrong, F. A.; Sykes, A. G.; Harrington, P. C.; Wilkins, R. G. *Biochim. Biophys. Acta* **1981**, *670*, 377−384.
(45) Zhang, M.; van Eldik, R.; Espenson, J. H.; Bakac, A. *Inorg. Chem.* **1994**, *33*, 130−133.
(46) Becker, M.; Schindler, S.; van Eldik, R. *Inorg. Chem.* **1994**, *33*, 5370−5371.
(47) Projahn, H.-D.; Dreher, C.; van Eldik, R. *J. Am. Chem. Soc.* **1990**, *112*, 17−22.

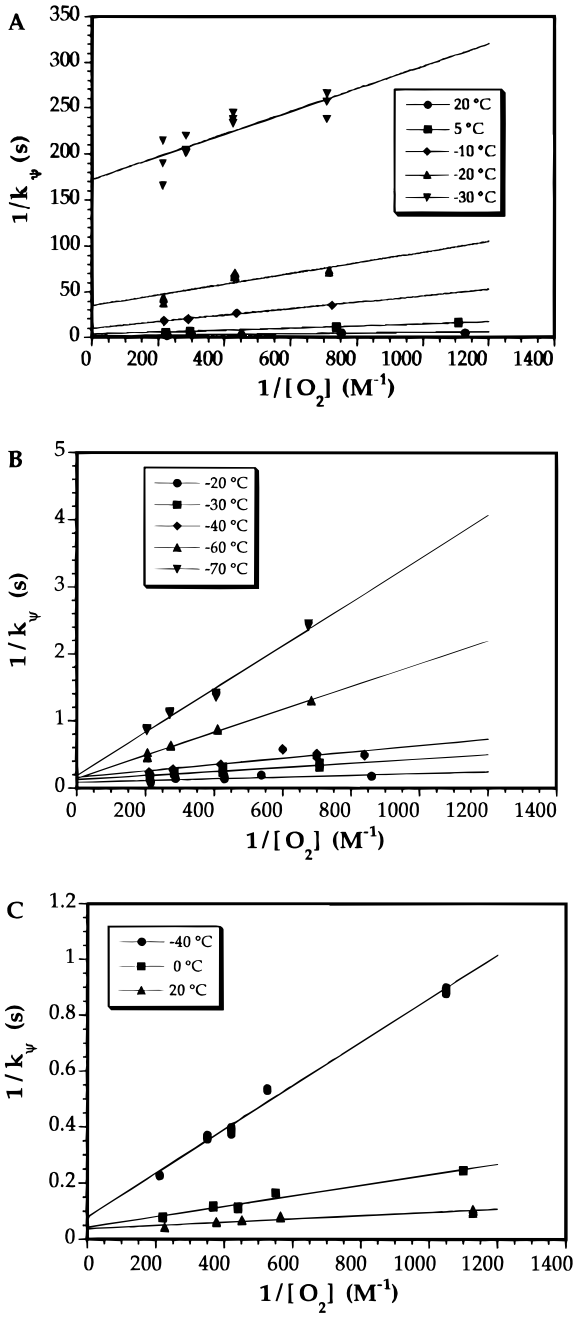

Figure 4. Double-reciprocal analysis for the formation of **1b** (A), **2b** (B), and **3b** (C) based on eqs 11 and 12. Data were collected between −70 and +20 °C and at dioxygen concentrations between 0.1 and 0.48 mM. Data at each temperature were fit to a linear least-squares regression (solid lines).

Eyring plot in Figure 5 assumes that the interaction of **1a** with O_2 is an elementary reaction with a single barrier. The situation has already been shown to be more complicated, however. By use of the rate constants derived from the slopes and intercepts of Figure 4A at each temperature, the effective activation barriers for the two phases of the reaction can be separated. These values have different meanings, however, depending on which model is used to define the mechanism. In the case of eqs 9−11, the activation parameters derived from the intercepts in Figure 4A correspond to k_0, the forward reaction rate constant in a ligand rearrangement equilibrium, whereas the model in eqs 12−14 indicates that this value corresponds to the reversible addition of dioxygen to the ferrous complex. The entropy of activation derived from these intercepts is negative, a result which supports the interpretation of the mechanism outlined in eqs 12−14. The

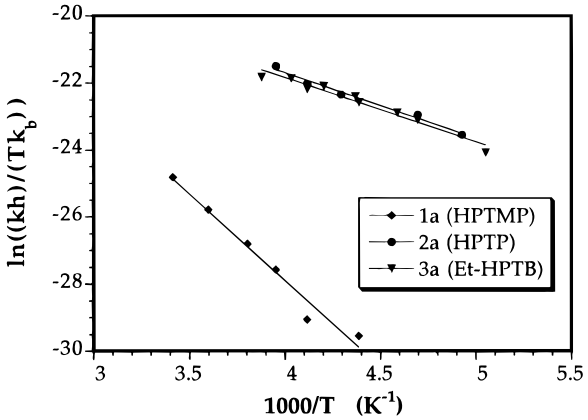

Figure 5. Eyring plot for the reaction of 0.16−0.25 mM **1a** (diamonds), **2a** (circles), and **3a** (triangles) with ≈4.4 mM dioxygen in propionitrile based on the observed second-order rate constants between −70 and +20 °C.

binding of dioxygen in this step has a very large enthalpy of activation for an associative reaction, however, and is more in keeping with a bond-breaking step.

Effect of Pressure on the Rate of Oxygenation. The effect of pressure on the rate of **3b** formation was studied in propionitrile between 10 and 140 MPa (Figure 6 and Table S11). From eq 18,[48] we computed the volume of activation to be

$$\left(\frac{\partial(\ln k)}{\partial P}\right)_T = -\frac{\Delta V^{\ddagger}}{RT} \qquad (18)$$

-12.8 ± 0.9 cm^3 mol^{-1} at 20 °C, a value consistent with the simple addition mechanism discussed above. Efforts to measure the volumes of activation for the formation of **1b** and **2b** were not successful because of technical limitations of the high-pressure stopped-flow system, which was unable to access sufficiently low temperatures to study the reaction efficiently.

Effect of Water on the Rate of Oxygenation. When **1a** crystallized from MeOH/H_2O, water coordinated to one of the iron atoms.[29] We therefore studied the effect of added water on the rate of formation of the peroxide intermediates. Reaction of **3a** was investigated, because its greater thermal stability allowed work at higher temperatures and therefore higher water concentrations. At temperatures of −30 °C and below, ice crystals formed in aqueous propionitrile solutions at the higher end of the water concentration range, resulting in light scattering and the inability to collect useful data. The addition of up to 1% (v/v) water (0.5 M) at 20 °C had no effect on the reaction rate (Figure S1A and Table S12), indicating that if water was ligated, as it was in the solid state, it was readily displaced by dioxygen. An interesting observation during this study was that the extinction coefficient of the peroxide complex increased linearly by up to 60% over the range of water concentrations studied (Figure S1B).

Decomposition of the Diferric Peroxo Species 1b−3b. The complexes formed initially from the reaction of dioxygen and compounds **1a**−**3a** are all metastable. When kept sufficiently cold, they survive indefinitely. The three compounds have quite different decomposition rates and temperature sensitivities, however.[28,30] The most stable adduct is **3b**, which survives for minutes to hours at room temperature depending on the concentration and is completely stable below −35 °C. The least stable is **2b**. An initial report indicated that this peroxide adduct did not even form at room temperature.[30] The statement is,

(48) van Eldik, R.; Merbach, A. E. *Comments Inorg. Chem.* **1992**, *12*, 341−378.

Table 2. Activation Parameters for Formation and Decay of Peroxide Intermediates **1b**−**3b** and Other Relevant Protein and Model Systems

	$\Delta H^{\ddagger}$ [a] (kJ mol^{-1})	$\Delta S^{\ddagger}$ [a] (J mol^{-1} K^{-1})	$\Delta V^{\ddagger}$ (cm^3 mol^{-1})	$\Delta H^{\ddagger}$[b] (kJ mol^{-1})	$\Delta S^{\ddagger}$[b] (J mol^{-1} K^{-1})
		Oxygenation Reactions			
1a → **1b**	42.2 ± 1.6	−63 ± 6		39.6 ± 2.4	−114 ± 9
				39.2 ± 1.6	−65 ± 6
2a → **2b**	16.5 ± 0.4	−114 ± 2			
3a → **3b**	15.4 ± 0.6	−121 ± 3	−12.8 ± 0.9		
$LCu^{I} \rightarrow LCu^{II}(O_2)$			−21 ± 1[c]		
$LCo^{II} \rightarrow LCo^{II}(O_2)$			+0.4 ± 0.5[d]		
Hr → oxyHr[e]	16.8	−46	+13.3 ± 1.1[f]		
Mb → oxyMb			+5.2 ± 0.5[g]		
		Peroxide Decomposition Reactions			
1b → **1c**	113.3 ± 7.7	187 ± 27			
2b → **2c**	51.9 ± 2.7	−47 ± 11			
3b → **3c**	80.6 ± 3.9	74 ± 14		370 ± 6	−8 ± 12
				80.2 ± 7.0	73 ± 24
MMO[h]					
peroxo → Q	111	147			
Q → decay	75	8			

[a] Activation parameters in this column are derived from Eyring plots of observed rate constants (Figures 6 and S2). [b] Activation parameters for **1a** in this column correspond to values derived from the slope (top value) and intercept (bottom value) of the double-reciprocal analysis in Figure 5A. Based on the model in eq 17; the top value relates to k_1' and the bottom value $k_1'K_0$. For **3b**, the activation parameters correspond to k_3 (top vlaue) and K_3k_2' (bottom value) derived from Figure S3. [c] Data taken from ref 47. [d] Data taken from ref 46. [e] From *Themiste zostericola* in Tris buffer, pH 8.2, I = 0.1 M.[45] [f] From *T. zostericola* in Tris buffer, pH 8.5, I = 0.10 M.[57] [g] From sperm whale in Tris buffer, pH 8.5, I = 0.1 M.[48] [h] From *Methylococcus capsulatus* (Bath) in MOPS buffer, pH 7.0, I = 25 mM in the presence of protein **B**.[20]

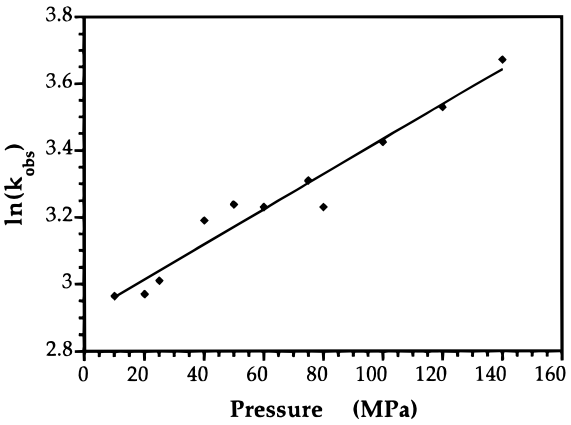

Figure 6. Plot showing the effect of pressure on the reaction of 0.20 mM **3a** with dioxygen between 10 and 140 MPa.

strictly speaking, incorrect, but the adduct decomposes so rapidly at this temperature that its blue color cannot be visually detected. At −77 °C, **2b** is quite stable. Compound **1b** was reported correctly to have stability properties between these two extremes.[28] Addition of polar aprotic cosolvents such as DMSO significantly stabilizes acetonitrile solutions of **2b** and **3b**,[30] but a detailed investigation of these effects was beyond the scope of the present study.

We first consider the stoichiometry of the decomposition reaction. As noted above, the diiron(II) compounds react in a 1:1 ratio with dioxygen to form peroxo intermediates. The original reports on compounds **2b** and **3b** noted that iron(III) decomposition products formed upon warming and that, at best, substoichiometric oxygen atom transfer occurred when good O atom acceptors such as triphenylphosphine were present.[30] By carrying out more detailed manometric studies, we were able to establish the stoichiometry shown in Scheme 1. Dioxygen uptake was first monitored at low temperature, after which the reaction vessel was allowed to warm to room temperature. The net number of moles of dioxygen consumed by all three compounds after completion of the decomposition reaction, however, was half the amount taken up during the initial low-temperature reaction step (Table 1). In other words, half of the dioxygen initially consumed to form the peroxide adduct was released following decomposition. We therefore write the decay reaction as a disproportionation that yields 1 equiv of dioxygen and either 2 equiv of a dinuclear ferric complex or 1 equiv of a tetranuclear species (Scheme 1). Mixed-isotope studies using $^{16}O_2$ and $^{18}O_2$ showed that no $^{16}O-^{18}O$ formed during decomposition.

Nature of the Final Oxidation Products. The studies reported here use the optical absorbance of the peroxo intermediate to analyze its decay, and therefore do not reflect subsequent reactions. In Scheme 1, we depict the products **1c**−**3c** as tetranuclear species, the structure of **3c** having been crystallographically determined.[11] Moreover, an X-ray study of the dinuclear ferric system $[Fe_2O(HPTB)(OBz)](NO_3)_2$, where HPTB is identical to Et-HPTB but lacks the *N*-ethyl groups, similarly revealed aggregation of two dinuclear units to form a tetranuclear species.[49] We therefore assign the structures of **1c**−**3c** as indicated in the scheme, but recognize that the initial product of the decomposition may be dinuclear.

Rate Laws for the Decay of the Peroxide Intermediates 1b−**3b.** A series of experiments systematically varying the concentrations of dioxygen and diiron(II) complexes was undertaken in a manner analogous to that described above for the formation of the intermediates, except that the temperatures used for these studies were higher to promote faster decomposition. The traces for this phase of the reaction fit to second-order decay equations, providing the first indication that the process was bimolecular. As shown in Figure 7 (see also Tables S13−S15), the reactions all have a second-order dependence on the concentration of the peroxide intermediate.

The reaction order with respect to dioxygen was a little more difficult to extract from the data. The effect of varying the dioxygen concentration is shown in Figure 8 (see also Tables S16−S18). The simplest case is the decomposition of **3b**, in which the reaction is clearly independent of the amount of dioxygen added. This result derives from the large difference between the rates of formation, which is O_2 dependent, and decay of **3b**. By the time the decay begins, the reaction of **3a** with O_2 to form **3b** is complete. Therefore, the formation of the peroxide adduct has no observable effect on the kinetics of

(49) Chen, Q.; Lynch, J. B.; Gomez-Romero, P.; Ben-Hussein, A.; Jameson, G. B.; O'Connor, C. J.; Que, L., Jr. *Inorg. Chem.* **1988**, *27*, 2673−2681.

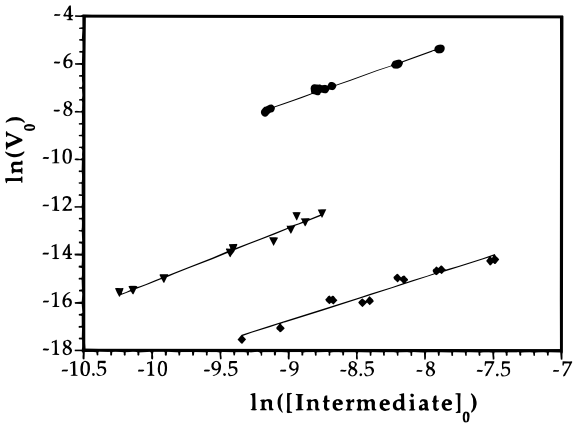

Figure 7. Reaction order plot showing the $\ln(V_0)$ for peroxide intermediate decomposition versus ln([**1b**,**2b**,**3b**]), the concentration at which second-order decomposition is observed to begin: **1b**, diamonds; **2b**, circles; **3b**, triangles.

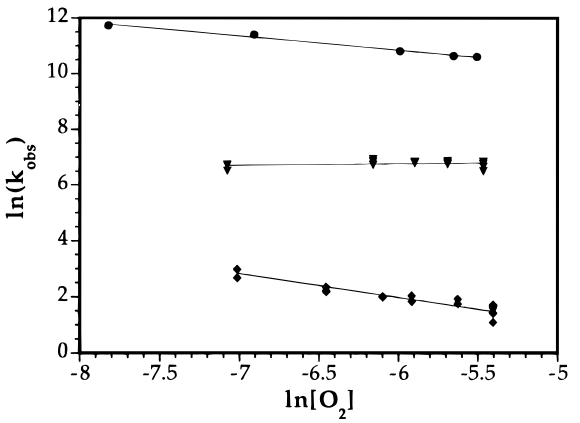

Figure 8. Reaction order plot showing the effect of $[O_2]$ (0.2−4.4 mM) on the observed second-order rate constant for the decay of peroxide intermediates **1b** (5 °C, diamonds), **2b** (22 °C, circles), and **3b** (55 °C, triangles); 0.15−0.75 mM.

the decay phase. For **1b** and **2b**, the separation of the two phases is less distinct. Since the kinetics are followed by using the optical band of the intermediate, no suitable absorptions being present in the spectra of the reaction products, a partial negative reaction order with respect to dioxygen is measured. This result derives from the formation of the peroxide discussed above and does not relate to the actual decomposition step. A minimal rate law describing this decay reaction is given by eq 19. By combination of the two phases of the reaction, the rate law in eq 20 can be written, the integrated form of which is

$$-\frac{d[\mathbf{B}]}{dt} = k_2[\mathbf{B}]^2 \tag{19}$$

$$\frac{d[\mathbf{B}]}{dt} = k_1[\mathbf{A}][O_2] - k_2[\mathbf{B}]^2 \tag{20}$$

shown in eq 6 above. One could add an additional term, $-k_{-1}[\mathbf{B}]$, assuming a back-reaction to re-form the diiron(II) starting material. In these intermediate regimes, however, satisfactory fits were obtained without such a term, showing that, from a kinetic standpoint, it was insignificant under the conditions studied.

Activation Parameters for the Decomposition of 1b−3b. The temperature dependence of the decomposition reaction was studied in propionitrile over a wide range, 80 °C for **2b** and, because of the slower decomposition rates, 50 °C for **1b** and **3b** (Figure S2 and Tables S19−S21). The activation enthalpies vary from 52 kJ mol^{-1} for **2b** to 113 kJ mol^{-1} for **1b**, a more significant deviation than was observed for the oxygenation phase. A surprising feature is the dramatic difference in activation entropy of 250 J mol^{-1} K^{-1} for the three reactions. Although the enthalpic variation is large, the large entropy changes clearly determine the relative stabilities of these intermediates. This feature is discussed in detail below.

In a final kinetic experiment, we investigated whether the rate law analogous to that outlined in eq 19 applies to the decay of all three compounds. To obtain this information, the complex concentration was varied at different temperatures. For the simplest case of eq 19, a single elementary reaction applies and the activation parameters are invariant. More complex behavior is indicated by changes in either $\Delta H^{\ddagger}$ or $\Delta S^{\ddagger}$, in which case a double-reciprocal analysis analogous to eq 16 or 17 must be used. The activation parameters for the decomposition of **1b** and **2b** were invariant over a concentration range of 0.12−1.00 mM. The same could not be said for **3b**, however. Assuming that a pre-equilibrium step was involved, similar to the behavior of the oxygenation of **1a**, $(k_{obs})^{-1}$ was plotted against $[\mathbf{3b}]^{-1}$ and a linear correlation was found at each temperature (Figure S3 and Table S22.). This more complex system can therefore be described by the reaction scheme and rate laws given in eqs 21−24.

$$\mathbf{B} \underset{k_{-3}}{\overset{k_3}{\rightleftharpoons}} \mathbf{B}' \tag{21}$$

$$\mathbf{B} + \mathbf{B}' \xrightarrow{k_2'} \mathbf{C} \tag{22}$$

$$-\frac{d[\mathbf{B}]}{dt} = \frac{k_3 k_2'[\mathbf{3b}]^2}{k_{-3} + k_2'[\mathbf{3b}]} \tag{23}$$

$$\frac{1}{k_{obs}} = \frac{1}{k_3} + \frac{k_{-3}}{k_3 k_2'[\mathbf{3b}]} \tag{24}$$

Discussion

The Role of Steric Factors in the Oxygenation Reaction. The three model compounds studied here are structurally quite similar (Scheme 1). The donor atoms of the dinucleating ligand are identical, and each complex has an additional benzoate bridge. Each iron atom is five-coordinate with an open binding site for dioxygen. The four pendant donor nitrogen atoms derive from slightly different residues, pyridyl, 6-methylpyridyl, and *N*-ethylbenzimidazolyl, all of comparable basicity. Despite these similarities, the kinetic behaviors of these three compounds in their reactions with dioxygen are substantially different.

Three parameters can be used to define the dioxygen-binding pockets in **1a**−**3a**, diameter, depth, and capping potential. The diameter of the pocket is determined by the $[Fe_2(OR)(O_2CPh)]^{2+}$ core and is identical for the three complexes. The depth of the pocket is defined by the nature of the four pendant bases, specifically the size of the aromatic rings which create it. Compound **3a** has a deeper pocket than **1a** and **2a** because of the fused rings of the benzimidazole moieties. Ligands having quinoline rings have been employed to provide extra pocket depth to pyridine-like bases in copper(I)−dioxygen reaction chemistry.[41] Finally, partial capping of the pocket is effected by the methyl groups of the HPTMP ligand (Figure 9).

These structural features, rather than minor electronic differences, most likely account for the kinetic behavior of **1a**−**3a**. The vacant sites on the iron atoms lie within the pockets just described. The pocket dimensions of **3a** provide little to no obstruction to approach of a small ligand like O_2. The effect

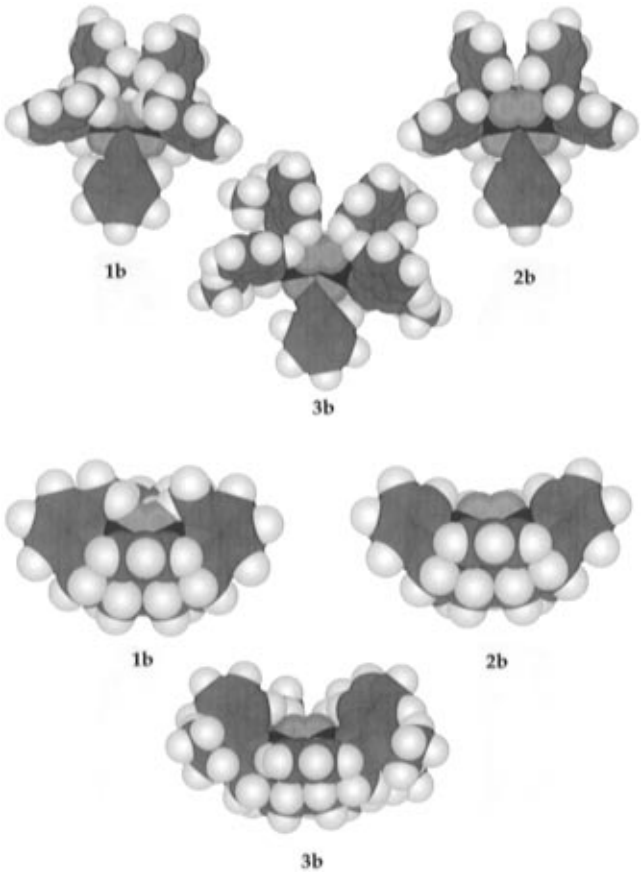

Figure 9. Space-filling models of **1b**−**3b** showing the dioxygen-binding site from two perspective views.

of capping by HPTMP is far more obstructive, however. There is a void space below these convergent groups which could accommodate a bridging peroxide ligand once it gets there (Figure 9). It is the process of accessing this compartment that differentiates the dioxygen reactions of these three systems. The decay of the peroxide intermediates is affected by a different parameter. Peroxo species **3b** decays much more slowly than **1b** or **2b**, and the temperature dependence of the reaction indicates that a dissociative step is important at lower temperatures. In this reaction, the relevant structural feature is the depth of the binding pocket (Figure 9). The fused rings of the benzimidazole groups of **3b** are substantially larger than the pyridyl arms of **1b** and **2b**, resulting in a deeper well and greater protection of the bound peroxide from bimolecular decomposition.

Comparison of the Mechanism of Formation of 1b to That of 2b and 3b. The temperature-dependent results most clearly illustrate the contrast in mechanism for the reactions of dioxygen with **1a** compared to either **2a** or **3a**. Both the diminished order in dioxygen and the behavior of **1a** shown in Figure 4 can be explained by the two-step mechanisms in eqs 9−14. In the first scenario, eqs 9−11, a ligand dissociation equilibrium is invoked. There are two chemically reasonable possibilities for the **1a** ⇌ **1a′** equilibrium. One is a carboxylate shift,[50] a process previously implicated in the oxidation chemistry of coordinatively saturated diiron(II) complexes[51] and known to accompany redox state changes of the diiron centers in both sMMO hydroxylase and RNR.[8,52,53] The steric difference between **1a** and the other two compounds is that the putative dioxygen-binding site is blocked by partial methyl group capping. The shift from bridging to terminal carboxylate coordination does not directly afford a passageway for dioxygen-binding, however, unless, in the process, additional ligand rearrangement occurs. This motion contrasts with the carboxylate shift reactions postulated in the oxidation of $[Fe_2(OH)(O_2CCH_3)_2(Me_3TACN)_2](ClO_4)$, where the shift directly provides a dioxygen binding site.[51] Dissociation of a pyridyl arm is the other alternative. The steric barrier to dioxygen approach to the metal center provided by the four methyl groups would be relieved by partial or complete dissociation of one of these arms. Iron(II) is a rather labile metal, and the dissociation rates for any single arm are likely to be quite rapid.[54] The complex as a whole is stabilized by the chelate effect, which implies that, statistically, it is unlikely for more than one arm to dissociate at a given time.

If either of the foregoing proposals is correct, the same type of behavior should be occurring for **2a** and **3a**. The difference is that, for these compounds, the dioxygen-binding step is not affected and the kinetics of adduct formation do not reflect the process. This point is important, for it implies inner-sphere coordination prior to, or concomitant with, the rate-determining step in the oxidation to form peroxide adducts. For a series of capped cyclidene iron(II) complexes, complicated kinetic changes accompanied the O_2 binding process when the cavity was constricted to a size which prevented O_2 access.[55,56] It was proposed that, under such conditions, autoxidation proceeded by an outer-sphere electron transfer mechanism. Compound **1a** is unreactive with dioxygen over a period of hours below −77 °C in propionitrile. Brief exposure to higher temperatures followed by cooling results in the formation of stable **1b**. An outer-sphere mechanism for autoxidation therefore appears not to be accessible in the present systems, or if it is, it must occur on a time scale longer than that investigated.

The scenario in eqs 12−14 offers a second possible mechanism to account for the kinetic results. In this case, an iron−dioxygen adduct other than the μ-1,2-peroxo species **1b** must exist as an intermediate. Such a species could contain a terminal superoxide ligand coordinated in a monodentate fashion to one iron in a mixed-valent core. This adduct might form in the case of **1a** oxidation because of steric constraints. For reasons discussed above, access to the vacant binding site is inhibited. Terminal coordination might anchor the dioxygen molecule in place as additional ligand motion ensues to allow access to the second iron atom and peroxide formation.

These two possible mechanisms can in principle be differentiated by the activation parameters derived from the slopes and intercepts of the double-reciprocal plots. In the case of eqs 9−11, these parameters correspond, respectively, to a composite constant (K_0k_1') and a unimolecular ligand rearrangement rate constant (k_0). In the second case, eqs 12−14, the parameters represent (K_0k_1') and a rate constant for the unimolecular rearrangement of **1a**·O_2 to **1b**. The $\Delta S^{\ddagger}$ value is negative in both plots (Table 2 and Figure S4), which implies a highly ordered transition state. This result favors a bimolecular process, and for this reason, we slightly prefer the latter model. The large enthalpy of activation implies that bond stretching or breaking is probably involved upon approach to this transition state, which can arise from the need to alleviate the steric constraint imposed by the partial capping of the binding site.

(50) Rardin, R. L.; Tolman, W. B.; Lippard, S. J. *New J. Chem.* **1991**, *15*, 417−430.
(51) Feig, A. L.; Masschelein, A.; Bakac, A.; Lippard, S. J., Manuscript in preparation.
(52) Rosenzweig, A. C.; Nordlund, P.; Takahara, P. M.; Frederick, C. A.; Lippard, S. J. *Chem. Biol.* **1995**, *2*, 409−418.
(53) Åberg, A. Ph.D. Thesis, Stockholm University, 1993.
(54) Porterfield, W. W. *Inorganic Chemistry—A Unified Approach*; Academic: New York, 1993.
(55) Sauer-Masarwa, A.; Dickerson, L. D.; Herron, N.; Busch, D. H. *Coord. Chem. Rev.* **1993**, *128*, 117−137.
(56) Busch, D. H.; Alcock, N. W. *Chem. Rev.* **1994**, *94*, 585−623.

Interpretation of the Activation Parameters for Adduct Formation and Comparisons to Other Systems. The activation parameters of a reaction reflect the transition state, allowing deductions about the reaction coordinate and comparisons to other known reactions to be made. Theoretically, the Eyring equation is valid only for elementary reactions. When more complicated reactions are subjected to such an analysis, negative curvature in the plot can be encountered, indicating that two separate steps are rate-limiting at the temperature extremes. In practice, however, it is often possible to study complex rate equations by this methodology so long as curvature is absent over a given temperature range. The values then correspond to the energy barrier for the rate-determining elementary step in that range. The Eyring plot shown in Figure 5 exemplifies such behavior for the reaction of **1a** with dioxygen. Over the temperature range studied, a single step dominates the activation barrier and a linear plot results. The reactions of **2a** and **3a** are simple second-order reactions, studied under pseudo-first-order conditions, and linearity is predicted.

The activation enthalpy for the reactions of **2a** and **3a** with dioxygen is remarkably similar to that of deoxyHr formation. It is possible that this agreement is merely a coincidence, but it may represent the energy barrier to reach the transition state in the interaction of dioxygen with a reduced diiron(II) center having an accessible binding site to form a peroxodiiron(III) species. In Hr, one iron atom has such a vacant site. Since the structures of the peroxide adducts differ for Hr and the model compounds, the implication is that the binding of dioxygen and the associated two-electron oxidation of the iron center comprise the rate-determining step. Structural rearrangements to form a (μ-1,2-peroxo)diiron(III) intermediate in the case of the models, or the terminal hydroperoxide with a hydrogen-bond to the oxo-bridge in Hr, might be subsequent, kinetically silent, steps.

The measured value of -12.8 cm^3 mol^{-1} for the activation volume of the reaction is another parameter which confirms, along with the negative value of the activation entropy, the highly structured nature of the transition state. Strongly negative volumes of activation (≈ -20 cm^3 mol^{-1}) were also reported for the reaction of copper(I) complexes with O_2.[46,57] These values were interpreted in terms of bond formation accompanied by intramolecular electron transfer to produce the $Cu^{II}-O_2$ species. By contrast, volumes of activation for the binding of dioxygen to macrocyclic cobalt(II) complexes were close to zero and interpreted in terms of a substitution-controlled binding process.[45] In the case of the dioxygen carrier proteins myoglobin, hemocyanin, and hemerythrin, the volumes of activation for the binding of dioxygen differ significantly from those reported above due to influence of the protein environment.[47,58]

Solvent Effects. Since water binds to **1a**,[28] it could potentially affect the kinetics of the oxygenation reaction by blocking a binding site. Extensive studies with added water, however, showed no significant effect on the kinetic parameters for oxidation of **3a** in the 2.0−500 mM range. Exploratory work in acetonitrile and $CHCl_3$ similarly failed to reveal any dramatic changes. The absolute rates were slightly slower, a factor of 2−3, in $CHCl_3$, consistent with a passive role for solvent in these reactions. A significant effect on the extinction coefficient of **3b** was observed as a function of water concentration. The linear dependence of this effect indicated that it did not arise from water coordination, which would have a hyperbolic form similar to that encountered in an acid−base titration. The changes in optical density therefore do not relate to a binding event.

Two Possible Peroxo Intermediate Decay Mechanisms. The results for decay of the peroxide intermediates provide some interesting clues about the behavior of these metastable species. This reaction is of primary interest to those seeking to understand non-heme iron oxo-transfer chemistry. It is this step in the overall transformation which diverts small-molecule model compounds from mimicking the chemistry of the sMMO and R2 active sites. As already discussed, the model compounds form peroxide intermediates similar to those found in the native protein systems, and they do so with analogous activation parameters provided that the diiron center is sterically accessible. Yet these same models cannot activate substrates or perform catalysis. The reason for this behavior is apparent from the kinetics of the decay reactions, which are second-order with respect to complex. In order for a catalyst to generate a highly energetic intermediate with enough oxidizing potential, for example, to break a C−H bond, all lower energy pathways leading to autoxidation must be avoided. The bimolecular reaction uncovered here is one such pathway, knowledge of which should facilitate the development of strategies to avoid it.

We now consider the nature of the peroxide decomposition step. In work with two other model compounds, $[Fe_2(OH)(O_2CCH_3)_2(Me_3TACN)_2](ClO_4)$ and $[Fe_2(O_2CH)_4(BIPhMe)_2]$, we proposed a ($\mu_4$-peroxo)diiron(II)diiron(III) transition state.[51] Such an activated complex would probably arise by a different mechanism for peroxide intermediates **2b** and **3b** for two reasons. One relates to the apparent irreversibility of their formation. Once dioxygen reacts with the diiron(II) compounds, it is impossible to reverse this process at low temperature, even in vacuum down to 10^{-3} Torr. Even warming a solution of **2b** or **3b** under vacuum does not regenerate **2a** or **3a**. The second reason is based on the relative rates of the formation and decay of the peroxo intermediates, especially **3b**. The half-lives of the two phases of the reaction differ by 4−5 orders of magnitude depending on complex concentration. By the time **3b** begins to decompose, no **3a** is available as a reactant. For **1a**, however, the reaction with dioxygen is reversible, with a $P_{1/2}$ of 6 Torr at -35 °C in CH_2Cl_2.[28] Although this binding is reasonably strong, it is possible that the second-order decomposition results from reversal of the oxygenation step followed by reaction of another equivalent of the peroxo intermediate with the resultant **1a**. Given the similarity of the three compounds, however, it is likely that the decomposition reactions follow similar pathways, with the only perturbations arising from different steric constraints.

Since a mechanism in which an equivalent of the peroxide adduct reacts with the diiron(II) starting material seems unlikely under our conditions (excess O_2 in solution), two possibilities remain for the decomposition reaction. These possibilities are presented in Scheme 2. Both fit the kinetic data, resulting in second-order decay reactions with the loss of an equivalent of dioxygen. The first pathway (A) is analogous to the decay of secondary and tertiary alkyl peroxide radicals, which proceeds through a tetraoxide intermediate.[59−61] Following decomposition, an equivalent of alcohol, an equivalent of ketone, and a molecule of dioxygen are formed. The other mechanism (B) involves more conventional nucleophilic attack and disproportionation. Mechanism A was evaluated by the $^{16}O_2/^{18}O_2$-labeling experiment discussed above. Since a new O−O bond forms in the decomposition step, the central two

(57) Goldstein, S.; Czapski, G.; van Eldik, R.; Cohen, H.; Meyerstein, D. *J. Phys. Chem.* **1991**, *95*, 1282−1285.
(58) Projahn, H.-D.; Schindler, S.; van Eldik, R.; Fortier, D. G.; Andrew, C. R.; Sykes, A. G. *Inorg. Chem.* **1995**, *34*, 5935−5941.
(59) Bartlett, P. D.; Guaraldi, G. *J. Am. Chem. Soc.* **1967**, *89*, 4799−7801.
(60) Bartlett, P. D.; Günther, P. *J. Am. Chem. Soc.* **1966**, *88*, 3288−3294.
(61) Traylor, T. G.; Bartlett, P. D. *Tetrahedron Lett.* **1960**, 30−36.

Scheme 2

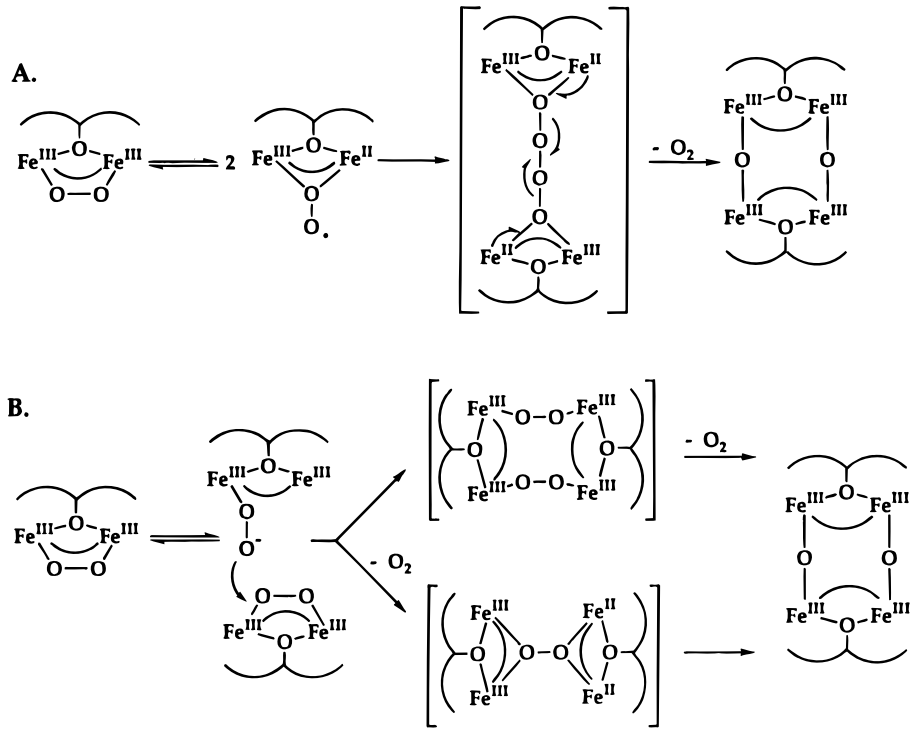

oxygen atoms of the tetraoxide depart as O_2. In the O_2-labeling experiment, where **3b** and **3b*** were mixed, degassed, and allowed to decompose under vacuum, no $^{16}O-^{18}O$ was recovered. Mechanism A can therefore be excluded, provided that an immeasurable but kinetically competent quantity of the diiron(II) starting material did not form. In mechanism B, the dioxygen molecule released following decomposition is one taken up during the first phase of the reaction. No O−O bonds are formed during the reaction. Because dioxygen is released after a rate-determining, second-order process in mechanism B, it is impossible to determine whether this process occurs immediately or occurs in a subsequent step. Both possibilities are depicted in Scheme 2B.

The bottom pathway in Scheme 2B would provide a common intermediate for the decay pathway presented here and the one proposed previously.[51,62] A (μ_4-peroxo)tetrairon adduct has been crystallographically characterized.[63] In this molecule, there are only Fe(III) centers instead of the $Fe^{II}_2Fe^{III}_2$ transition state postulated here. As mentioned above, loss of dioxygen from **2b** and **3b** was not observed even under vacuum. The energy barrier for the back-reaction thus appears to be greater than that for the decomposition. During the bimolecular collision, however, the kinetic energy of the two molecules might lead to a species with sufficient vibrational potential energy that O_2 dissociation is observed. Once O_2 is released, newly formed diiron(II) material would be able to react rapidly with a molecule of the peroxo intermediate to lead to product formation.

Relation of the Kinetic Parameters to the Chemical Properties of the Compounds. The stability of the peroxide adducts **1b**−**3b** is a property of considerable interest, since these species are analogs of the biological precursors to high-energy intermediates which oxygenate substrates at the active sites of dinuclear non-heme iron enzymes. The bimolecular decay reaction observed here is prevented from occurring in the protein because the peroxodiiron(III) species is secluded deep within a folded polypeptide. The measured activation parameters for the bimolecular reaction, however, provide a measure of the instability of the protein intermediates even though the decay mechanisms differ. A model compound will decompose by the lowest energy pathway, regardless of whether it is unimolecular or bimolecular. If the transition state energies for the two pathways are comparable, then both reactions will occur in parallel. The kinetic traces in such cases would appear biphasic, the sum of first-order and second-order decays. Therefore, the activation enthalpies presented here for the bimolecular reaction provide a lower limit for a comparable, unobserved unimolecular mechanism.

A reaction coordinate diagram reflecting the experimentally determined activation parameters is presented in Figure 10. Not all of the information necessary for constructing this diagram was available, so approximations were made. For **1a**, the value of $P_{1/2}$ for dioxygen binding is known (6 Torr at −35 °C)[28] and corresponds to a ΔG value of −9.6 kJ mol^{-1}. Although the temperature dependence of the binding has not been reported, a crude approximation of 80 J mol^{-1} K^{-1} can be made based on the measured values reported for Hr.[64] The ΔG values for the decomposition of the peroxide intermediates were chosen arbitrarily, but since the reactions are irreversible, the importance of the **c** → b activation barriers is minimal. The reactions of **2a** and **3a** with dioxygen cannot be reversed by the application of vacuum. One may therefore conservatively set an upper limit on dioxygen binding at $P_{1/2} \leq 0.05$ Torr. This inequality leads to an upper bound of $\Delta G < -19$ kJ mol^{-1} for **2a** and **3a**, the value used in preparing Figure 10. The depth of the wells containing **2b** and **3b** could be substantially greater than actually shown. Microcalorimetry experiments would be useful to determine these energies. Even by using the maximum values for ΔG it can be seen that formation of **2b** is unlikely to be reversible at accessible temperatures. The potential for observ-

(62) Liu, K. E.; Feig, A. L.; Goldberg, D. P.; Watton, S. P.; Lippard, S. J. In *The Activation of Dioxygen and Homogeneous Catalytic Oxidation*; Barton, D. H. R., Ed.; Plenum: New York, 1993; pp 301−320.

(63) Micklitz, W.; Bott, S. G.; Bentsen, J. G.; Lippard, S. J. *J. Am. Chem. Soc.* **1989**, *111*, 372−374.

(64) De Waal, D. J. A.; Wilkins, R. G. *J. Biol. Chem.* **1976**, *251*, 2339−2343.

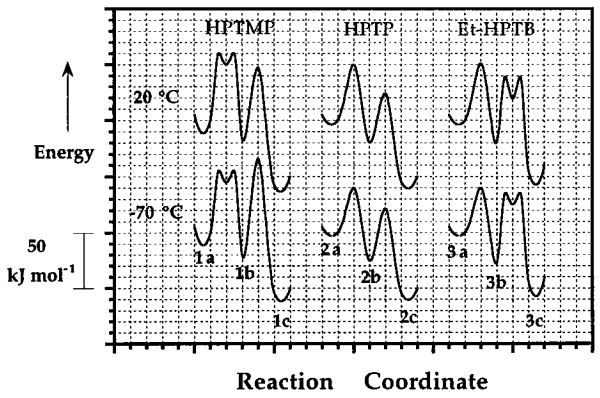

Figure 10. Reaction coordinate diagram showing $\Delta G^{\ddagger}$ for the reactions of **1a**−**3a** with dioxygen at +20 and −70 °C.

ing reversibility with **3b** is somewhat greater, but again the ΔG value for **3b** formation could be substantially more favorable than actually depicted.

The formation of **1b** and the decay of **3b** are not elementary steps, although linear behavior in an Eyring plot was observed. The shallow wells shown as part of the transitions from **1a** to **1b** and from **3b** to **3c** (Figure 10) represent the intervening steps discussed above. The heights of the net barriers for the reactions have been measured, but the two component steps contributing to the overall transformations have not been delineated.

The variation in the activation parameters among the three peroxide intermediates reveals the primary difference in their stabilities to be entropic. For **1b** and **3b** decomposition, $\Delta S^{\ddagger}$ is large and favorable. Such a finding is unusual for a bimolecular event where the transition state is usually more ordered than the reactants. There are two potential explanations for this behavior. One is that $\Delta S^{\ddagger}$ reflects solvent reorganization. The reactants are divalent cations and will be highly solvated. On approaching the transition state, charge increases to +4. This process changes the surface-to-volume ratio of the charged species and could release many solvent molecules, contributing to a large positive increase in the entropy of activation. Addition of DMSO has been reported to stabilize the peroxo adducts, especially **2b**.[30] Altering the nature of this solvation might exert very significant effects on the entropic term. The second, more likely, possibility is that the transition state involves release of 1 equiv of dioxygen (Scheme 2B, bottom pathway). Such a mechanism would offset the effect of a bimolecular collision, and there would be no change in the net number of species.

In all three cases, the activation enthalpy for decomposition of the peroxide adduct is a factor of 3−5 greater than that for its formation. The relative values of the activation entropy for the forward (k_2) and reverse (k_{-1}) reactions therefore dictate the relative decomposition rates. In addition, ΔG for converting diferrous material to the peroxide adduct plays a key role in determining the reversibility of the reaction. This value affects the depth of the well in which the intermediate resides (Figure 10) and therefore the partition ratio between the forward reaction and back reaction. The relatively high energy of **1b** most likely reflects steric interactions between dioxygen and the methyl groups in the pocket it occupies (Figure 10).

Destabilization of the peroxide intermediate in this manner leads to an interesting possibility which goes against current dogma for rationalizing reversible dioxygen binding. In the case of Hr, it has been proposed that the peroxide adduct is stabilized by hydrogen bonding and that this interaction somehow prevents its decomposition by pathways normally observed for sMMO and RNR. In the present model systems, however, the ground state of the reversible binder is higher than that of the intermediates which undergo only irreversible decomposition. By formation of a dioxygen adduct which is too stable, the barrier to reversibility cannot be overcome and only forward pathways leading to the cleavage of the O−O bond are observed. Other systems such as the cyclidenes and capped porphyrins also bind dioxygen reversibly. It is possible that such a ground state effect operates in these cases too. The diiron centers in RNR and sMMO have vacant coordination sites on both iron atoms and the formation of a 1,2-bridging peroxide has been proposed in each case. Such a peroxide intermediate may be too low in energy to undergo O_2 release and therefore is committed to a pathway leading to dioxygen activation.

Summary and Conclusions

The dioxygen uptake and subsequent decomposition reactions for three diiron(II) model compounds have been studied by stopped-flow spectroscopy. The mechanistic results show that two of the models accurately mimic the oxygenation chemistry of Hr. When sufficient ligand steric constraints prevent efficient access to the diiron(II) center by the incoming dioxygen molecule, a two-step mechanism is required to explain the kinetic data. This process could involve a pre-equilibrium involving a ligand dissociation process or, more likely, the intermediate reversible formation of a dioxygen adduct other than the symmetrically coordinated peroxide. This species could be a terminal superoxide adduct. The key steric factor affecting the addition of dioxygen to the diferrous compounds was identified as capping of the binding site (compound **1a**).

Thermal decomposition of the peroxide intermediates occurs in all three cases by a nonbiomimetic second-order rate-determining step. In this reaction, an equivalent of dioxygen is evolved such that the stoichiometry of the overall transformation is 0.5 equiv of O_2 per dinuclear center, similar to that observed for reactions of other non-heme diiron model compounds with dioxygen.[51] In order for efficient biomimetic oxygenation of substrates to occur, this second-order decay reaction must be subverted. The trends observed for these three compounds reveal that, whereas capping is important for the O_2-binding step, the depth of the coordination pocket plays a more significant role in the decomposition reactions. The stability of the μ-1,2-peroxide intermediates studied here indicates that such species are not likely to be the species directly responsible for oxygen transfer in the enzymes. This statement implies either that O−O bond cleavage occurs prior to C−H activation or that the dioxygen adduct isomerizes to a more activated form prior to its interaction with a substrate in monooxygenase reactions.

Acknowledgment. This work was supported by grants from the National Institute for General Medical Science, the AKZO Corp., and the Deutsche Forschungsgemeinschaft. We wish to thank V. L. Pecoraro and A. Bakac for interesting discussions.

Supporting Information Available: Tables S1−S22, containing kinetic constants used in preparing the figures, and Figures S1−S4 (26 pages). Ordering information is given on any current masthead page.

IC951242G